Highly dispersed FeOOH to enhance photocatalytic activity of TiO_2 for complete mineralisation of herbicides

*Ayoola Shoneye and Junwang Tang**

Department of Chemical Engineering, University College London

Torrington Place, London, WC1E 7JE, UK.

*To whom correspondence should be addressed.

E-mail: *junwang.tang@ucl.ac.uk (Prof. J. Tang).*

Abstract

Although there were many new photocatalysts reported recently, TiO_2 has still been considered as one of the best candidates for real application of environmental decontamination. Fe-based oxides were synthesised as efficient and equally important non-toxic active species to improve the efficiency of TiO_2 photocatalysts. Such nano-architectured FeO_x/TiO_2 was tested for herbicides mineralisation e.g. 2,4,6-trichlorophenol (2,4,6-TCP) and 2,4-dichlorophenoxyacetic

acid (2,4-D) under full arc light irradiation. The consistent results were achieved by HPLC, TOC and UV-vis spectra measurements, which show among three Fe species, $Fe_4NO_3(OH)_{11}$, FeOOH and Fe_2O_3, FeOOH is the best to improve TiO_2 activity. This active specie of FeOOH was readily controlled by synthesis temperature and precursor concentration, leading to 250 ^oC being the optimum temperature for the synthesis of very stable FeOOH/TiO_2 nanocomposite with excellent photocatalytic activity, representing nearly two times activity of the benchmark PC50 TiO_2 photocatalyst for all herbicides tested. Such high activity was attributed to the enhanced photo-generated electron-hole separation and improved generation of hydroxyl radicals by FeOOH. The multifunction of FeOOH is very crucial for organic pollutants mineralisation. The mechanistic studies also show that degradation of 2,4,6-TCP was mostly dominated by hydroxyl radicals and superoxide radicals. The possible degradation pathway of 2,4,6-TCP was also proposed.

Keywords

mineralisation, iron, photocatalyst, TiO_2, water treatment

1. Introduction

The presence of toxic and persistent organic pollutants in wastewater effluents causes serious environmental problems [1, 2]. Chlorophenols (CPs) and derivatives are common and recalcitrant environmental pollutants believed to have high bioaccumulation capability, carcinogenic and mutagenic effects [2 – 4]. However CPs and their derivatives find extensive application in the chemical, forestry, and wood-working industries. They are used as herbicides, insecticides, fungicides, wood preservatives and chemical intermediates [3]. Generally, these organic pollutants are released into the environment because of several man-made activities

including water disinfection, waste incineration, uncontrolled used of pesticides and herbicides, and as by-products in the bleaching of paper pulp with chlorine [2]. The Environmental Protection Agency (EPA) recommended maximum allowable concentration for chlorinated phenols is 0.1 μg/L in drinking water and 200 μg/L in wastewater (EPA 2003) [2, 5].

Various strategies have been employed to remove organic and inorganic contaminants from the environment. Conventional methods include coagulation-flocculation [6], reverse osmosis [7], active carbon adsorption [8], biodegradation [9], air stripping [10] and incineration [11]. However, these techniques have some drawbacks and limitations e.g. toxic by-product generation, incomplete mineralisation, low efficiency, high energy and capital cost [3, 12 – 14]. Chlorophenols absorb light of wavelength below 290 nm, thus they do not undergo direct sunlight photolysis [15]. Therefore, it is important to find innovative and cost-effective techniques for the safe and complete degradation of chlorinated organic pollutants such as chlorophenols.

TiO_2 based materials have been the most studied photocatalysts for the degradation of various chlorophenols e.g. 2-CP, 4-CP, 2,4-DCP and 2,4,6-TCP [16]. Several TiO_2 based photocatalysts e.g. Ag-doped TiO_2 [17], Fe-doped TiO_2 [18, 19], La-doped TiO_2 [20], V_2O_5/TiO_2 [21] and other photocatalysts like ZnO [22 – 24], α-Bi_2O_3 [25], Ag_3PO_4 [26], $BiVO_4$ [27] and g-C_3N_4 [28 – 30] have also been reported for the degradation of 2,4,6-TCP in aqueous solution. However, photocatalyst stability and/or mineralisation efficiency (not decomposition efficiency) are the major challenges encountered during degradation of 2,4,6-TCP. Due to this drawback of the doped TiO_2 and non-TiO_2 photocatalysts for the degradation of chlorinated phenols, extensive research is still required to develop a cheap, non-toxic, photo-chemically stable and highly efficient TiO_2-based photocatalyst for scalable wastewater purification.

The surface modification of TiO_2 with Fe(III) species as co-catalysts has been reported due to its high efficiency and robust synthesis procedure, unlike doping into TiO_2 lattice which requires a very high temperature [31, 32]. It has been reported that the use of low Fe(III) concentration in TiO_2 surface modification typically led to the formation of isolated ions or clusters of Fe(III) species [33, 34]. The Fe(III) species that accepted photogenerated electrons got reduced to Fe(II) species, which were unstable and would easily be oxidised back to Fe(III) through oxygen reduction reaction [34]. The photocatalytic enhancement contributed by Fe_2O_3 clusters has been broadly investigated in the literature and assigned to the interfacial charge transfer (IFCT) from TiO_2 to Fe(III) or cross excitation from TiO_2 to Fe species [35 - 38]. However, the active Fe species to improve the photocatalytic activity of TiO_2 was mainly regarded as Fe_2O_3 or ferric oxide [35 - 46]. Production of reactive oxygen species and reduction of charge recombination during mineralisation of organic pollutants are important in photocatalytic water treatment.

Herein, we report the synthesis of novel nano-architecture comprising different phases of Fe(III) species on PC50 (commercial anatase TiO_2), using a reproducible surface impregnation method. The active species of $Fe_4NO_3(OH)_{11}$, FeOOH and Fe_2O_3 were found to be readily controlled by synthesis temperature. The Fe(III) species were thoroughly characterised in order to clarify their functionality and actual active species. The degradation of 2,4,6-TCP in water was carried out under full arc light irradiation. The effects of co-catalyst concentration, choice of Fe(III) precursor and calcination temperature were investigated. The charge transfer mechanism and the reaction pathway were also discussed. Photocatalytic mineralisation ability of the optimised catalyst was also evaluated with another widely used herbicide, 2,4-dichlorophenoxyacetic acid (2,4-D) to demonstrate its wide feasibility.

2. Experimental Section

2.1. Chemicals

PC50 TiO_2 (purely anatase) was purchased from Millennium chemicals. 2,4,6-trichlorophenol (98%) was purchased from Alfa Aesar. 2,4-dichlorophenoxyacetic acid was purchased from Cayman Chemical Company. 1,4-benzoquinone (99%) was purchased from Acros Organics. $Fe(NO_3)_3 \cdot 9H_2O$, $FeCl_3 \cdot 6H_2O$, $Fe_2(SO_4)_3 \cdot H_2O$, DMPO and EDTA (99%) were purchased from Sigma-Aldrich. Isopropanol (HPLC grade), KHP and Acetonitrile (HPLC grade) were purchased from Fischer Scientific. All reagents were used as received without further purification.

2.2. Sample preparation

Fabrication of $FeOOH/TiO_2$

A modified surface impregnation and drying technique was used to fabricate $FeOOH/TiO_2$ and Fe_2O_3/TiO_2 composites [47]. In a typical experiment, the appropriate percentage weight of iron (III) nitrate nonahydrate was added to an aqueous suspension of 1.0 g of commercial PC50 TiO_2 in a clean alumina crucible under mild stirring, with Fe/TiO_2 composition range (0.07 to 2.8 wt.% Fe). The obtained slurry was continuously stirred with a magnetic stirrer bar and dried slowly at 80 ^oC on a hotplate. The resultant dried powder was hand-milled and calcined in a muffle furnace under air atmosphere at 250 ^oC for 4 hours during study on effect of Fe loading on photocatalytic activity. The sample prepared at this temperature was denoted as $FeOOH/TiO_2$ as proved by XRD and Raman characterisation. It was collected after cooling down to room temperature, hand-ground again and stored for photocatalytic activity

tests and characterisations. Subsequent study on the choice of Fe(III) precursor (nitrate, sulphate and chloride) was evaluated using optimum Fe loading (0.14 wt.%), followed by a study on the effect of calcination temperature (120 to 450 ºC).

2.3. Characterisation of photocatalysts

High resolution X-ray photoelectron spectroscopy (XPS) was performed using a Thermo Scientific K-alpha photoelectron spectrometer using monochromatic Al kα radiation; peak positions were calibrated to carbon (284.5 eV) and plotted using the CasaXPS software. Powder X-Ray Diffraction (PXRD) measurements were performed using a STOE StadiP diffractometer in foil mode with Mo kα radiation (λ = 0.071 nm, 50 kV, 30 mA) and a Bruker D4 diffractometer in reflection geometry with Cu kα radiation (λ = 0.154 nm, 40 kV, 30 mA). Specific surface area (S.A) measurements were performed using the BET method (N_2 adsorption, TriStar 3000, Micrometrics). The morphologies of the products were characterised using TEM (JEOL 2010F) with EDS detector. Raman scattering and photoluminescence (PL) were measured using a Renishaw 1000 Raman microscope with 514 nm and 325 nm excitation lasers at room temperature, respectively. In situ electron spin resonance (ESR) signals of radicals trapped by DMPO (5,5'-dimethyl-1-pyrroline-N-oxide) were obtained using MS-5000 Magnettech ESR spectrometer.

2.4. Photocatalytic measurements

A 300 W Xe lamp (Newport) was used as the light source with a plain glass window (λ > 320 nm) as a cut-off filter. The glass window shields all UV light with wavelength < 320 nm. In a typical measurement, 0.1 g of photocatalyst was suspended in 200 mL 50 ppm aqueous

132 solution of 2,4,6-TCP or 25 ppm aqueous solution of 2,4-D in de-ionised water. The suspension
133 was sonicated in an ultrasonic water-bath for 15 mins and then magnetically stirred in the dark
134 for 1 h to achieve adsorption/desorption equilibrium of herbicides on the photocatalyst. The
135 suspension was then exposed to light irradiation ($\lambda > 320$ nm) and the reaction vessel was
136 immersed in a water-bath to regulate temperature ($T \leq 30$ ^{o}C). Upon irradiation, 3 mL aliquot
137 was withdrawn at regular time intervals and filtered through a micropore syringe filter (PTFE,
138 0.2 μm) before further analysis.
139
140 **2.5. Analyses**
141 The photocatalytic activity of the prepared TiO_2 samples towards herbicides
142 mineralisation was investigated primarily using a Shimadzu total organic carbon (TOC-L)
143 analyser after calibration with potassium hydrogen phthalate (KHP) as a primary standard. The
144 change in herbicide concentration was measured using a high performance liquid chromatograph
145 (HPLC-2030C, Shimadzu) consisting of a binary pump, an autosampler, a photodiode array
146 detector and an ACE-5 C18 (5μm × 150 mm × 4.6 mm) reverse phase column maintained at 40
147 ^{o}C. The HPLC used a 5 – 95% gradient (Acetonitrile/H_2O with 0.1% formic acid) as the mobile
148 phase. The flow rate was set at 1.0 mL/min and the injection volume was 20 μL. The initial
149 mobile phase was 5% A (acetonitrile) and 95% B (water containing 0.1% formic acid) and kept
150 isocratic for 1 min, followed by a linear gradient to 95% A in 15 min, and kept isocratic for 3
151 min, and then back to 5% A in 0.5 min. A UV-vis spectrophotometer was also used to monitor
152 herbicides degradation rate with the optimised sample for comparison. Intermediate products
153 formed during herbicide mineralisation were detected using a single quadrupole tandem mass

spectrometer (Shimadzu 2020 series LC-MS system), equipped with an electrospray ionisation (ESI) source. The MS detection was operated in negative ionisation mode.

3. Results and discussion

3.1. Characterisation of FeOx/TiO_2 nanocomposites

The XRD patterns of unmodified PC50 TiO_2 and the selected FeOOH/TiO_2 samples with varying Fe concentration are shown in **Fig. 1a**. Typical diffraction peaks corresponding to anatase (JCPDS 21-1272) are observed in these samples. No characteristic diffraction peaks of Fe-related species (e.g. Fe, FeO, FeOOH, $Fe(OH)_x$, Fe_2O_3 or Fe_3O_4) are observed on the surface modified TiO_2. This could be due to the highly dispersed and low amount of iron species loaded on TiO_2 and the intensive background signal caused by TiO_2. The absorption spectra of unmodified PC50 TiO_2 and as-prepared FeOOH/TiO_2 nanocomposites are shown in **Fig. 1b**. There is a slight change in band-gap for low Fe samples (0.07 - 0.7 wt.%) samples compared to unmodified PC50 TiO_2 (ca. 3.2 eV), indicating low amount of Fe contributes little to the light absorption of the nanocomposites. With increasing Fe loading (up to 2.8 wt.%), there is a significant red shift in light absorption and lowering of the nanocomposites band-gap to ca. 2.2 eV, which is due to visible light absorption from the Fe(III) species on TiO_2 surface.

High resolution XPS was used to identify the Fe species present in the FeOOH/TiO_2 samples. Fe 2p peaks are not observed in the XPS survey spectrum of the 0.14 wt.% Fe sample (**Fig. 1c**), which is due to the low amount of Fe loading and high dispersion on TiO_2. The Fe 2p

peaks are observed after increasing the Fe concentration to 1.4 wt.% (**Fig. 1c**). Peaks corresponding to Fe^{3+} are confirmed around 711 eV (Fe $2p^{3/2}$) and 724 eV (Fe $2p^{1/2}$) in the Fe 2p XPS spectrum of 1.4 wt.% Fe sample and no peaks are observed for the 0.14 wt.% Fe sample (**Fig. 1d**). This could also be due to the low Fe loading in the sample and the intensive background signal caused by Ti 2p and O 1s signals of TiO_2 [47]. Absence of a peak at 709 eV rules out the presence of Fe^{2+} in the FeOOH/TiO_2 nanocomposites [48]. From the N1s scan in **Fig. S1**, residual nitrogen species, which were absent in the PC50 TiO_2, could be slightly detected on the surface of FeOOH/TiO_2 (0.14 wt.% Fe) sample. Furthermore, for N 1s scan, a single peak observed around 407 eV corresponds to NO_3^- species as reported in literature [49].

The XRD patterns of 0.14 wt.% Fe/TiO_2 samples, calcined at different temperatures are shown in **Fig. 2a**. Typical diffraction peaks corresponding to anatase (JCPDS 21-1272) are also observed in all samples. The diffraction peaks relating to Fe species could not be identified here. This could again be due to the highly dispersed and low concentration of Fe species and intensive background signal caused by TiO_2. The UV-vis absorption spectra of 0.14 wt.% Fe/TiO_2 nanocomposites calcined at different temperatures are shown in **Fig. 2b**. There is no significant shift in the light absorption band-edge for all samples. The TEM image in **Fig. 2c** reveals the average particle size of the anatase TiO_2 to be approximately 20 – 30 nm but the Fe (III) species could not be imaged directly at this low Fe concentration. This is due to the high dispersity of Fe species on TiO_2 as shown in the EDS elemental mapping for Fe and Ti (**Fig. S2**). From the Raman spectra in **Fig. 2d**, the characteristic Raman frequencies 399 cm^{-1} (B_{1g}), 519 cm^{-1} (A_{1g}) and 639 cm^{-1} (E_{1g}) corresponding to anatase are observed [50], while the peaks relating to Fe species could not be observed.

To investigate the impact of calcination temperature on the physical properties of the modified samples, BET surface area measurements were carried out and results are displayed in **Table 1**. From the results, there appears to be little variation in surface area from unmodified PC50 TiO_2 to the sample calcined at 450 ºC. This implies that the moderate surface impregnation method neither reduced the surface area of PC50 nor significantly increased the surface area.

3.2. Photocatalytic activity

The calibration curve for the TOC analyser using KHP standard solutions is displayed in **Fig. 3a** and it shows a good linear fit (r^2 = 0.9999). Photocatalytic activities of the as-prepared FeOOH/TiO_2 composites were first evaluated by the mineralisation of 2,4,6-TCP under full arc light irradiation (λ > 320 nm), as shown in **Fig. 3b**. Virtually 0% TOC removal was observed after 4 h of light irradiation in the absence of photocatalyst. Similar observation was recorded from the UV-vis absorption spectra measurements in **Fig. S3** since the glass window shields all UV light with wavelength < 320 nm. The adsorption-desorption equilibrium of 2,4,6-TCP on the photocatalyst was achieved in 30 mins as shown in **Fig. S4**. The peak at 292 nm was monitored since the shoulder peak at 310 nm is very sensitive to slight changes in solution pH as confirmed in **Fig. S5**. This phenomenon could be due to protonation/deprotonation of the O-H group in TCP [23].

The TCP mineralisation rate recorded by PC50 TiO_2 is nearly 50% after 4 h. Approximately 71% TOC removal is achieved with FeOOH/TiO_2 (0.07 wt.% Fe) sample after 4 h. An increase in Fe concentration up to 0.14 wt.% Fe led to a further increase in photocatalytic activity, while poor TCP mineralisation rates are observed with 1.4 and 2.8 wt.% Fe-loaded

222 samples. The optimum condition for the preparation of FeOOH/TiO_2 nanocomposites was found
223 to be 0.14 wt.% Fe with ca. 90% TOC removal after 4 h, nearly doubling the benchmark
224 photocatalyst PC50 activity. Co-catalyst loading of 0.42 and 0.7 w.t% Fe also display close
225 photocatalytic activity as the optimised sample in **Fig. 3c**. However, a significant reduction in the
226 photocatalytic mineralisation efficiency is observed with higher Fe concentration (2.8 wt.% Fe),
227 compared to unmodified PC50 TiO_2 after 4 h test. Generally, co-catalyst is required to improve
228 the photocatalytic degradation rate due to enhanced charge separation and catalytic effect, while
229 increasing the amount of co-catalyst over the optimum adversely affects the photocatalytic
230 activity, which was also reported in literature [51 – 53]. This observation could be due to
231 shielding of intrinsic light absorption by colorful co-catalysts and occupying the oxidation sites
232 on TiO_2 [47].

233 Furthermore, to investigate the contribution of the choice of Fe(III) precursors,
234 FeOOH/TiO_2 (0.14 wt.% Fe) was prepared using other low cost Fe precursors (sulphate and
235 chloride). From the results in **Fig. 3d**, there is no significant difference in photocatalytic
236 mineralisation activities of the three samples. However, the composite prepared from Fe(III)
237 nitrate has a slight edge after 240 mins as observed from the TOC measurements, thus Fe(III)
238 nitrate was used again as Fe precursor for subsequent experiments.

239 The effect of calcination temperature was investigated with optimised Fe/TiO_2 composite
240 (0.14 wt.% Fe loading). The highest photocatalytic activity was observed with the sample
241 prepared at 120 ^oC. Nearly complete 2,4,6-TCP mineralisation (100% TOC removal) was
242 achieved in 4 h run, as shown in **Fig. 4a**, and about 15% higher than the FeOOH/TiO_2 sample
243 prepared at 250 ^oC. The FeOOH/TiO_2 is 40% more active than Fe_2O_3/TiO_2 prepared at 350 ^oC,
244 while the latter is still better than pure TiO_2 as we earlier reported [45]. An increase in

calcination temperature beyond 350 ºC negatively affects the photocatalytic activity of the nanocomposites. The worst is the sample calcined at 450 ºC, with only about 35% TOC removal in 4 h run. The uncertainty of optimised FeOOH/TiO_2 is shown in **Fig. 4b** after carrying out the mineralisation experiment in triplicates. The result signifies that the experiment is repeatable to a large extent. Such enhancement in activity of the sample calcined at both 120 ºC and 250 ºC might have some contribution from defects on FeOOH cocatalyst. Also, FeOOH could improve the adsorption of organic contaminants on TiO_2 as reported [32].

In order to evaluate 2,4,6-TCP degradation rate, a calibration curve (**Fig. S6**) was plotted using measurements from an HPLC system. The PDA detector wavelength was set at 292nm and it shows a good linear fit (r^2 = 0.998). The corresponding temporal HPLC chromatograms for 2,4,6-TCP degradation with optimised FeOOH/TiO_2 are displayed in **Fig. S7**. The TCP degradation process follows typical pseudo-first-order kinetics on both samples (**Fig. S8**) [24]. The initial rate constant for the optimised FeOOH/TiO_2 sample was calculated to be 0.0193 min^{-1}, which is 3 times that of unmodified PC50 TiO_2 (0.00647 min^{-1}). **Fig. 4c** shows a comparison between unmodified TiO_2 and FeOOH/TiO_2 (0.14 wt.% Fe) for 2,4,6-TCP degradation. Nearly 50% and 90% degradation rates are achieved in 2 h with the unmodified TiO_2 and optimised FeOOH/TiO_2 sample, respectively.

2,4,6-TCP removal with optimised FeOOH/TiO_2 was also analysed with a UV-vis spectrophotometer and compared with results obtained from TOC and HPLC analyses, as shown in **Fig. 4d**. The UV-vis result tends to be less accurate when compared with measurements from HPLC. This could be due to interference of colorless intermediate products at the monitored wavelength (292 nm) for TCP degradation. In 120 min, TOC shows approximately 60% of organic substance still exists, while HPLC indicates 90% of 2,4,6-TCP was converted so the

mineralisation efficiency is notably less than the degradation efficiency due to the generation of organic intermediates during photocatalysis.

The poor TCP mineralisation rates recorded for the samples calcined at 350 and 450 ºC are not related to the BET surface area of the samples (**Table 1**) and light absorption ability (**Fig. 2b**). This implies that the nature of Fe(III) species on TiO_2 is responsible for the disparity in photocatalytic degradation efficiency. The Fe(III) containing oxides were thus prepared without the substrate TiO_2 and evaluated for TCP degradation [32]. The results in **Fig. S9** show 0 and 10% TCP degradation efficiencies in 3 h are obtained by Fe_2O_3 sample prepared at 450 ºC and FeOOH prepared at 250 ºC, respectively, indicating the species FeOOH prepared at 250 ºC is rather active.

Further studies on photocatalytic mineralisation ability of the optimised FeOOH/TiO_2 sample was evaluated with a widely used herbicide, 2,4-dichlorophenoxyacetic acid (2,4-D) and results are displayed in **Fig. 5a**. 0% TOC removal is observed after 3 h of light irradiation in the absence of a photocatalyst. Similar observation was recorded from the UV-vis absorption spectra measurements (**Fig. S10**). Nearly 60% and 100% TOC removal are achieved with the unmodified TiO_2 and optimised FeOOH/TiO_2 sample, respectively. 2,4-D removal by the optimised FeOOH/TiO_2 was also analysed with HPLC and UV-vis spectra, shown in **Fig. 5b**. Similar to what is observed in **Fig.4d**, the UV-vis spectra results is less accurate when compared with measurements from HPLC, which is again due to interference of colorless intermediate products at the monitored wavelength (228 nm) for 2,4-D degradation.

Due to the difficulty in identifying the highly dispersed specific Fe(III) species on TiO_2, the iron precursor of large amount was used to prepare samples at different temperatures [32] (1 g of sample, calcined for 6 h) and the yield was sufficient for analysis using Raman spectroscopy

and XRD. The XRD patterns in **Fig. 6a** with enlarged XRD patterns of some selected samples (**Fig. 6b**) are matched with a reference database, and could give a clue to the likely Fe(III) species obtained at different calcination temperatures. Samples calcined at 350 and 450 ºC consist of hematite, Fe_2O_3 (JCPDS 33-0664), sample calcined at 250 ºC matches FeOOH (JCPDS 76-0182), while the sample calcined at 120 ºC is a mixture of Fe(III) species i.e., trace amount of $Fe_4NO_3(OH)_{11}$ (JCPDS 44-0520) and the major phase of FeOOH. From the Raman spectra in **Fig. 6c**, the samples calcined at 350 and 450 ºC exhibit the characteristic Raman shift peaks of hematite (Fe_2O_3) i.e. 293, 405 and 613 cm^{-1}, which are absent in the samples calcined at 120 and 250 ºC, and consistent with XRD analysis [54]. The Raman peaks of samples calcined at 120 and 250 ºC are left-shifted, with a characteristic peak around 390 cm^{-1} indicating FeOOH species [54]. Therefore, the presence of FeOOH species is the key here which enhanced the photocatalytic activity of the composites prepared at 120 ºC and 250 ºC. To investigate whether charge transfer is facilitated between TiO_2 and the Fe(III) species, photoluminescence (PL) measurements were carried out (**Fig. 6d**). Strong emission from bare TiO_2 is observed under 325 nm excitation but surprisingly, about 95% reduction in the emission intensity is observed with optimised FeOOH/TiO_2 sample calcined at 250 ºC. Although the samples exhibit similar band-gap absorption, this is a strong indication of the efficiency of charge separation and transfer between FeOOH and TiO_2. Therefore, the enhanced photocatalytic performance is attributed to the efficient charge separation and catalytic effect of FeOOH, which is more efficient than Fe_2O_3 as we earlier reported [45].

Stability test was also carried out on the best samples under similar operational conditions during photocatalytic degradation experiments, except for the increase in amount of photocatalyst powder to 0.5 g. The cycle tests were performed at three hours intervals. The

photocatalyst was recovered from solution via centrifugation method and re-used immediately for subsequent cycles without any pre-treatment or make-up. The graph in **Fig. 7a** shows normalised activities with TiO_2 as a reference, when taking into account the stable activity of pure TiO_2 (**Fig. S11**), the photocatalytic recyclability performance follows the order: 350 $^oC \approx$ 250 $^oC >$ 120 ^oC. This implies that at higher calcination temperature, more stable photocatalysts were produced, which might be due to a more intimate contact between the Fe(III) species and TiO_2 particles. The sample prepared at 250 ^oC ($FeOOH/TiO_2$) is quite stable unlike the sample prepared at 120 ^oC ($FeOOH + Fe_4NO_3(OH)_{11}/TiO_2$) which could likely be due to the presence of iron nitrate hydroxide impurities that could help catalytic effect of FeOOH but is not as stable as FeOOH. The lower photocatalytic degradation efficiency recorded for the 350 ^oC calcined sample, compared to others, is likely due to the conversion of FeOOH to Fe_2O_3 on TiO_2 surface [55]. Therefore, the best in terms of activity is 0.14 wt.% Fe/TiO_2 prepared at 120 ^oC, while taking into account both stability and activity, the optimised sample is the one prepared at 250 ^oC.

3.3. Photocatalytic mechanism and degradation pathway

It is generally accepted that the reaction pathways for photocatalytic degradation of organic water contaminants are dominated by several active species (e.g. holes, superoxide radicals and hydroxyl radicals) [46, 56]. Herein, some scavengers were utilised to confirm the active species, which will further assist in understanding the photocatalytic degradation mechanism for 2,4,6-TCP degradation, using the $FeOOH/TiO_2$ (0.14 wt.% Fe) sample. EDTA was used as hole (h^+) scavenger, isopropanol (IPA) as hydroxyl radical ($\cdot OH$) scavenger and 1,4-benzoquinone as superoxide radical ($\cdot O_2^-$) scavenger [57]. As shown in **Fig. 7b**, about 97% 2,4,6-

TCP degradation is recorded in 4 h without any additive. The degradation rate drops to about 70% in the presence of hole scavenger and about 20% with superoxide radical ($\cdot O_2^-$) scavenger, while virtually no activity is recorded with hydroxyl radical scavenger. This implies that the degradation of 2,4,6-TCP was mostly dominated by hydroxyl radicals and superoxide radicals. This observation is somewhat consistent with literature on other photocatalysts [29, 46, 57]. ESR technique was employed to monitor the enhancement in generation of these reactive oxygen species with DMPO as spin-trapping agent and results are shown in **Figs. S12** and **S13**. No ESR signals are detected when the reaction is carried out in the dark. Under full arc light irradiation (λ > 320 nm), the characteristic peaks of DMPO-$\cdot$OH and DMPO-$\cdot O_2^-$ adducts could be observed [39, 57, 58]. There is a significant improvement in the generation of hydroxyl radicals, while generation of superoxide radicals is not enhanced by the optimised FeOOH/TiO_2 compared to unmodified TiO_2 sample. This indicates that FeOOH enhanced the generation of hydroxyl radicals in the TiO_2 composite for complete mineralisation of 2,4,6-TCP.

During 2,4,6-TCP oxidative degradation, most researchers reported the generation of 2,6-dichloro-1,4-benzoquinone (2,6-DCBQ) as the first intermediate product, which is a light sensitive compound that can easily transform into a mixture of 2,6-dichlorohydroquinone (2,6-DCHQ) and 2,6-dichloro-3-hydroxy-1,4-benzoquinone (2,6-DCHBQ) under light irradiation [29, 59]. These intermediate products can be further degraded via the aromatic ring cleavage [60] and finally mineralised to give small molecules (aliphatic carboxylic acids) [61].

In this work, the degradation intermediates of 2,4,6-TCP were analysed by HPLC in tandem with LC-MS using ESI negative mode. Six intermediate products were detected as shown in **Figs. 8a-d** and **Fig. S14**. Peak 1 with retention time of 5.1 min and m/z values at 191, 193 could be assigned to 2,6-dichloro-3-hydroxy-1,4-benzoquinone (2,6-DCHBQ). Peak 2 with

retention time of 5.8 min and m/z values at 193, 195 could be assigned to 2,6-dichlorobenzene-1,3,4-triol (2,6-DCBT). Peak 3 with retention time of 7.3 min and m/z values at 177, 179 could be assigned to 2,6-dichlorohydroquinone (2,6-DCHQ). Peak 4 with retention time of 9.1 min and m/z values at 211, 213 could be assigned to 2,4,6-trichlororesorcinol (2,4,6-TCR). Peak 5 with retention time of 9.3 min and m/z values at 177, 179 could be assigned to 3,5-dichlorocatechol (3,5-DCC). Since 2,6-DCHQ and 3,5-DCC have similar m/z values, their assignment is in order of elution time as reported in literature. Peak 6 with retention time of 9.7 min could be assigned to 2,6-dichloro-1,4-benzoquinone (2,6-DCBQ). This intermediate product could not be detected with ESI-MS technique due to ionisation problems as reported in literature [62]. Finally, peak 7 with retention time of 11.5 min and m/z values at 195, 197 could be assigned to the model pollutant under investigation (2,4,6-TCP).

From the discussion above, the possible pathway for 2,4,6-TCP degradation and intermediates formation is shown in **Scheme 1**. This is consistent with the order in which the intermediate products were detected regarding reaction time as shown in **Figs. 8a** and **8c**. Furthermore, it is somewhat similar to previously reported degradation pathway for 2,4,6-TCP [29, 62].

The 2,4,6-TCP degradation mechanism by FeOOH/TiO_2 is illustrated in **Scheme 2**. When the photocatalyst is exposed to light, photo-generated electrons are excited from the valence band (VB) to the conduction band (CB) of TiO_2. The VB holes are transferred to the surface FeOOH sites and subsequently react with hydroxyl ions (OH^-) in water to produce OH radicals, which oxidise 2,4-,6-TCP to intermediate products before its mineralisation. The 2,4,6-TCP degradation mechanism by Fe_2O_3/TiO_2 is illustrated in **S.I (Scheme 3).** This involves the transfer of electrons (generated in TiO_2) to the Fe_2O_3 conduction band for oxygen reduction reaction

383 [45]. The photocatalytic degradation of 2,4,6-TCP on bare FeOOH is quite negligible, and the
384 poor photocatalytic activity of FeOOH/TiO_2 (2.8 wt.% Fe) is observed compared to unmodified
385 TiO_2 (**Figs. 3b** and **S9**). Although there is visible light absorption originating from FeOOH (**Fig.**
386 **1b**), FeOOH cannot be regarded as a good photocatalyst for water treatment.
387
388
389 **4. Conclusions**
390 In summary, facile and robust synthesis procedure was successfully used in decorating
391 PC50 TiO_2 nanoparticles with highly dispersed FeOOH, which plays a key role for efficient
392 photocatalytic herbicide decomposition. The Fe loading and properties in the composites were
393 thoroughly controlled by varying the Fe concentrations from 0.07 to 2.8 wt.% Fe and calcination
394 temperatures from 120 to 450 ºC, respectively. At 120 ºC, iron nitrate hydroxyl impurities and
395 FeOOH were impregnated on surface of TiO_2. FeOOH nanoparticles were the only decorating
396 species at 250 ºC, while at temperatures higher than 250 °C, Fe_2O_3 species dominated. The
397 highest photocatalytic 2,4,6-TCP mineralisation efficiency was achieved with the composite
398 calcined at 120 ºC, which is more than two times higher than the unmodified PC50 TiO_2,
399 indicating the $Fe_4NO_3(OH)_{11}$ could aid FeOOH towards 2,4,6-TCP degradation. The sample
400 calcined at 250 ºC (FeOOH/TiO_2) displayed both excellent photocatalytic mineralisation
401 efficiency (nearly double activity of PC50) and better photocatalytic stability after three
402 successive degradation cycles than the 120 ºC calcined sample. About 100% TOC removal was
403 also achieved in 3 h during the other herbicide 2,4-D photocatalytic mineralisation by optimised
404 FeOOH/TiO_2 sample. The widely reported Fe_2O_3 decorated TiO_2 sample exhibited worse
405 performances than that decorated by FeOOH. The enhanced photo-generated electron-hole
406 separation and the catalytic effect of FeOOH for enhanced generation of hydroxyl radicals led to

high photocatalytic degradation performance. The mechanistic studies demonstrate that the degradation of the herbicides was primarily controlled by hydroxyl radicals and superoxide radicals. Overall, this work is of importance in the fabrication of low-cost, efficient and robust photocatalysts for water treatment.

Acknowledgments

A. Shoneye acknowledges studentship from the Federal Scholarship Board (FSB), Nigeria. J. Tang acknowledges funding from the Royal Society-Newton Advanced Fellowship award (NA170422) and Leverhulme Trust grant (RPG-2017-122).

Notes

The authors declare no competing financial interest.

References

(1) J. Romão, G. Mul, Substrate Specificity in Photocatalytic Degradation of Mixtures of Organic Contaminants in Water, ACS Catalysis 6 (2016) 1254-1262.

(2) A. Olaniran, E. Igbinosa, Chlorophenols and other related derivatives of environmental concern: Properties, distribution and microbial degradation processes, Chemosphere 83 (2011) 1297-1306.

(3) M. Czaplicka, Sources and transformations of chlorophenols in the natural environment, Science of the Total Environment 322 (2004), 21-39.

(4) S. Al-Asheh, F. Banat, L. Abu-Aitah, Adsorption of phenol using different types of activated bentonites, Separation and Purification Technology 33 (2003) 1-10.

(5) US Department of Health and Human Services, Toxicological Profile for Chlorophenols, Atlanta, GA. ATSDR, 1999.

(6) Z. Su, T. Liu, W. Yu, X. Li, N. Graham, Coagulation of surface water: observations on the significance of biopolymers, Water Research 126 (2017) 144-152.

(7) N. Khanzada, S. Khan, P. Davies, Performance evaluation of reverse osmosis (RO) pre-treatment technologies for in-land brackish water treatment, Desalination 406 (2017) 44-50.

(8) B. Schreiber, V. Schmalz, T. Brinkmann, E. Worch, The Effect of Water Temperature on the Adsorption Equilibrium of Dissolved Organic Matter and Atrazine on Granular Activated Carbon, Environmental Science & Technology 41 (2007) 6448-6453.

(9) S. Woods, J. Ferguson, M. Benjamin, Characterization of chlorophenol and chloromethoxybenzene biodegradation during anaerobic treatment, Environmental Science & Technology 23 (1989) 62-68.

(10) H. Mahmud, A. Kumar, A bench scale study of removal of cyclohexane and naphtha components from water by membrane air-stripping process, Desalination 287 (2012) 216-219.

(11) E. Bani-Hani, M. Hammad, A. Matar, A. Sedaghat, K. Khanafer, Numerical analysis of the incineration of polychlorinated biphenyl wastes in rotary kilns, Journal of Environmental Chemical Engineering 4 (2016) 624-632.

(12) A. Karci, I. Arslan-Alaton, T. Olmez-Hanci, M. Bekbölet, Transformation of 2,4-dichlorophenol by H_2O_2/UV-C, Fenton and photo-fenton processes: Oxidation products and toxicity evolution, Journal of Photochemistry and Photobiology A: Chemistry 230 (2012) 65-73.

(13) J. Bandara, J. Mielczarski, A. Lopez, J. Kiwi, Sensitized degradation of chlorophenols on iron oxides induced by visible light, Applied Catalysis B: Environmental 34 (2001) 321-333.

(14) O. Carp, C. Huisman, A. Reller, Photoinduced reactivity of titanium dioxide, Progress in Solid State Chemistry 32 (2004) 33-177.

(15) D.F. Ollis, H. Al-Ekabi, Photocatalytic Purification and Treatment of Water and Air, Elsevier, Amsterdam, 1993.

(16) F. Li, P. Du, W. Liu, X. Li, H. Ji, J. Duan, D. Zhao, Hydrothermal synthesis of graphene grafted titania/titanate nanosheets for photocatalytic degradation of 4-chlorophenol: Solar-light-driven photocatalytic activity and computational chemistry analysis, Chemical Engineering Journal 331 (2018) 685-694.

(17) S. Rengaraj, X. Li, Enhanced photocatalytic activity of TiO_2 by doping with Ag for degradation of 2,4,6-trichlorophenol in aqueous suspension, Journal of Molecular Catalysis A: Chemical 243 (2006) 60-67.

(18) P. Vijayan, C. Mahendiran, C. Suresh, K. Shanthi, Photocatalytic activity of iron doped nanocrystalline titania for the oxidative degradation of 2,4,6-trichlorophenol, Catalysis Today 141 (2009) 220-224.

(19) L. Liu, F. Chen, F. Yang, Y. Chen, J. Crittenden, Photocatalytic degradation of 2,4-dichlorophenol using nanoscale Fe/TiO_2, Chemical Engineering Journal 181-182 (2012) 189-195.

(20) H. Peng, J. Cui, H. Zhan, X. Zhang, Improved photodegradation and detoxification of 2,4,6-trichlorophenol by lanthanum doped magnetic TiO_2, Chemical Engineering Journal 264 (2015) 316-321.

(21) E. Sinirtas, M. Isleyen, G. Soylu, Photocatalytic degradation of 2,4-dichlorophenol with V_2O_5-TiO_2 catalysts: Effect of catalyst support and surfactant additives, Chinese Journal of Catalysis 37 (2016) 607-615.

(22) N. Selvam, S. Jesudoss, P. Rajan, L. Kennedy, J. Vijaya, Comparative Investigation on the Photocatalytic Degradation of 2,4,6-Trichlorophenol Using Pure and M-Doped (M = Ba, Ce, Mg) ZnO Spherical Nanoparticles, Journal of Nanoscience and Nanotechnology 15 (2015) 5910-5917.

(23) U. Gaya, A. Abdullah, M. Hussein, Z. Zainal, Photocatalytic removal of 2,4,6-trichlorophenol from water exploiting commercial ZnO powder, Desalination 263 (2010) 176-182.

(24) S. Anandan, A. Vinu, T. Mori, N. Gokulakrishnan, P. Srinivasu, V. Murugesan, K. Ariga, Photocatalytic degradation of 2,4,6-trichlorophenol using lanthanum doped ZnO in aqueous suspension, Catalysis Communications 8 (2007) 1377-1382.

(25) S. Sood, A. Umar, S.K. Mehta, S.K. Kansal, α-Bi_2O_3 nanorods: An efficient sunlight active photocatalyst for degradation of Rhodamine B and 2,4,6-trichlorophenol, Ceramics International 41 (2015) 3355-3364.

(26) X. Chen, Y. Dai, X. Wang, J. Guo, T. Liu, F. Li, Synthesis and characterization of Ag_3PO_4 immobilized with graphene oxide (GO) for enhanced photocatalytic activity and stability over 2,4-dichlorophenol under visible light irradiation, Journal of Hazardous Materials 292 (2015) 9-18.

(27) H. Golmojdeh, M. Zanjanchi, M. Arvand, $BiVO_4$-Silica Composites Containing Cobalt Phthalocyanine Groups: Synthesis, Characterization and Application in Photodegradation of 2,4,6-Trichlorophenol, Photochemistry and Photobiology 89 (2013) 1029-1037.

(28) J. Yang, H. Chen, J. Gao, T. Yan, F. Zhou, S. Cui, W. Bi, Synthesis of Fe_3O_4/g-C_3N_4 nanocomposites and their application in the photodegradation of 2,4,6-trichlorophenol under visible light, Materials Letters 164 (2016) 183-189.

(29) H. Ji, F. Chang, X. Hu, W. Qin, J. Shen, Photocatalytic degradation of 2,4,6-trichlorophenol over g-C_3N_4 under visible light irradiation, Chemical Engineering Journal 218 (2013) 183-190.

(30) D. Ma, J. Wu, M. Gao, Y. Xin, T. Ma, Y. Sun, Fabrication of Z-scheme g-C_3N_4 /RGO/Bi_2WO_6 photocatalyst with enhanced visible-light photocatalytic activity, Chemical Engineering Journal 290 (2016) 136-146.

(31) M. Pelaez, N.T. Nolan, S.C. Pillai, M.K. Seery, P. Falaras, A.G. Kontos, P.S.M. Dunlop, J.W.J. Hamilton, J.A. Byrne, K. O'Shea et al., A Review on the Visible Light Active

Titanium Dioxide Photocatalysts for Environmental Applications, Appl. Catal. B Environ. 125 (2012) 331–349.

(32) G. Rao, H. Zhao, J. Chen, W. Deng, B. Jung, A. Abdel-Wahab, B. Batchelor, Y. Li, FeOOH and Fe_2O_3 Co-Grafted TiO_2 Photocatalysts for Bisphenol A Degradation in Water, Catal. Commun. 97 (2017) 125–129.

(33) Q. Jin, M. Fujishima, H. Tada, Visible-Light-Active Iron Oxide-Modified Anatase Titanium(IV) Dioxide, J. Phys. Chem. C 115 (2011) 6478–6483.

(34) S. Neubert, D. Mitoraj, S.A. Shevlin, P. Pulisova, M. Heimann, Y. Du, G.K.L. Goh, M. Pacia, K. Kruczała, S. Turner et al., Highly Efficient Rutile TiO_2 Photocatalysts with Single Cu(ii) and Fe(iii) Surface Catalytic Sites, J. Mater. Chem. A 4 (2016) 3127–3138.

(35) H. Tada, Q. Jin, H. Nishijima, H. Yamamoto, M. Fujishima, S.I. Okuoka, T. Hattori, Y. Sumida, H. Kobayashi, Titanium(IV) Dioxide Surface-Modified with Iron Oxide as a Visible Light Photocatalyst, Angew. Chem. Int. Ed. 50 (2011) 3501–3505.

(36) M. Liu, X. Qiu, M. Miyauchi, K. Hashimoto, Energy-Level Matching of Fe(III) Ions Grafted at Surface and Doped in Bulk for Efficient Visible-Light Photocatalysts, J. Am. Chem. Soc. 135 (2013) 10064–10072.

(37) H. Yu, H. Irie, Y. Shimodaira, Y. Hosogi, Y. Kuroda, M. Miyauchi, K. Hashimoto, Visible-Light-Active Iron Oxide-Modified Anatase Titanium(IV) Dioxide, J. Phys. Chem. C 114 (2010) 16481–16487.

(38) M. Liu, R. Inde, M. Nishikawa, X. Qiu, D. Atarashi, E. Sakai, Y. Nosaka, K. Hashimoto, M. Miyauchi, Enhanced photoactivity with nanocluster-grafted titanium dioxide photocatalysts, ACS Nano. 8 (2014) 7229–7238.

(39) H. Liu, H.K. Shon, X. Sun, S. Vigneswaran, H. Nan, Preparation and characterization of visible light responsive Fe_2O_3 -TiO_2 composites, Appl. Surf. Sci. 257 (2011) 5813–5819.

(40) B. Palanisamy, C.M. Babu, B. Sundaravel, S. Anandan, V. Murugesan, Sol-gel synthesis of mesoporous mixed Fe_2O_3/TiO_2 photocatalyst: Application for degradation of 4-chlorophenol, J. Hazard. Mater. 252–253 (2013) 233–242.

(41) H.H. Mohamed, N.A. Alomair, S. Akhtar, T.E. Youssef, Eco-friendly synthesized α-Fe_2O_3/TiO_2 heterojunction with enhanced visible light photocatalytic activity, J. Photochem. Photobiol. A Chem. 382 (2019) 111951

(42) D. Wodka, R.P. Socha, E. Bielanska, M. Elzbieciak-Wodka, P. Nowak, P. Warszynski, Photocatalytic activity of titanium dioxide modified by Fe_2O_3 nanoparticles, Appl. Surf. Sci. 319 (2014) 173–180.

(43) Q. Sun, W. Leng, Z. Li, Y. Xu, Effect of surface Fe_2O_3 clusters on the photocatalytic activity of TiO_2 for phenol degradation in water, J. Hazard. Mater. 229–230 (2012) 224–232.

(44) L. Cheng, S. Qiu, J. Chen, J. Shao, S. Cao, A practical pathway for the preparation of Fe_2O_3 decorated TiO_2 photocatalyst with enhanced visible-light photoactivity, Mater. Chem. Phys. 190 (2017) 53–61.

(45) S. Moniz, S. Shevlin, X. An, Z. Guo, J. Tang, Fe_2O_3-TiO_2 Nanocomposites for Enhanced Charge Separation and Photocatalytic Activity, Chemistry - A European Journal 20 (2014) 15571-15579.

(46) S. Lee, H. Lintang, L. Yuliati, High photocatalytic activity of Fe_2O_3/TiO_2 nanocomposites prepared by photodeposition for degradation of 2,4-dichlorophenoxyacetic acid, Beilstein Journal of Nanotechnology 8 (2017) 915-926.

(47) S. Neubert, P. Pulisova, C. Wiktor, P. Weide, B. Mei, D. Guschin, R. Fischer, M. Muhler, R. Beranek, Enhanced photocatalytic degradation rates at rutile TiO_2 photocatalysts modified with redox co-catalysts, Catalysis Today 230 (2014) 97-103.

(48) T. Yamashita, P. Hayes, Analysis of XPS spectra of Fe^{2+} and Fe^{3+} ions in oxide materials, Applied Surface Science 254 (2008) 2441-2449.

(49) J. Baltrusaitis, P. Jayaweera, V. Grassian, XPS study of nitrogen dioxide adsorption on metal oxide particle surfaces under different environmental conditions, Physical Chemistry Chemical Physics 11 (2009) 8295.

(50) T. Ohsaka, F. Izumi, Y. Fujiki, Raman spectrum of anatase, TiO_2, Journal of Raman Spectroscopy 7 (1978) 321-324.

(51) H. Huang, J. Lin, G. Zhu, Y. Weng, X. Wang, X. Fu, J. Long, A Long-Lived Mononuclear Cyclopentadienyl Ruthenium Complex Grafted onto Anatase TiO_2 for Efficient CO_2 Photoreduction, Angewandte Chemie 128 (2016) 8454-8458.

(52) C. Adán, A. Bahamonde, M. Fernández-García, A. Martínez-Arias, Structure and activity of nanosized iron-doped anatase TiO_2 catalysts for phenol photocatalytic degradation, Applied Catalysis B: Environmental 72 (2007) 11-17.

(53) K. Shimura, H. Kawai, T. Yoshida, H. Yoshida, Bifunctional rhodium cocatalysts for photocatalytic steam reforming of methane over alkaline titanate, ACS Catalysis 2 (2012) 2126-2134.

(54) D. de Faria, S.S. Venâncio, M. de Oliveira, Raman Microspectroscopy of Some Iron Oxides and Oxyhydroxides, Journal of Raman Spectroscopy 28 (1997) 873-878.

(55) L. Kong, C. Wang, F. Wan, H. Zheng, X. Zhang, Synergistic effect of surface self-doping and Fe species-grafting for enhanced photocatalytic activity of TiO2 under visible-light, Appl. Surf. Sci. 396 (2017) 26–35.

(56) Y. Cong, J. Zhang, F. Chen, M. Anpo, Synthesis and Characterization of Nitrogen-Doped TiO_2 nanophotocatalyst with High Visible Light Activity, The Journal of Physical Chemistry C 111 (2007) 6976-6982.

(57) L. Luo, A. Shoneye, D. Wang, J. Wang, X. Sun, J. Tang, F. Fu, J. Ma, H. Shen, W. Xue, Synergistic Effect of Surface Oxygen Vacancies and Interfacial Charge Transfer on Fe(III)/Bi_2MoO_6 for Efficient Photocatalysis, Appl. Catal. B Environ. 247 (2019) 150–162.

(58) W. Zhao, J. Zhang, X. Zhu, M. Zhang, J. Tang, M. Tan, Y. Wang, Enhanced nitrogen photofixation on Fe-doped TiO_2 with highly exposed (101) facets in the presence of ethanol as scavenger, Appl. Catal. B Environ. 144 (2014) 468–477.

(59) G. Lente, J.H. Espenson, Photoreduction of 2,6-Dichloroquinone in Aqueous Solution: Use of a Diode Array Spectrophotometer Concurrently to Drive and Detect a Photochemical Reaction, J. Photochem. Photobiol. A Chem. 163 (2004) 249–258.

(60) A. Sorokin, S. De Suzzoni-Dezard, D. Poullain, J.P. Noël, B. Meunier, CO_2 as the Ultimate

Degradation Product in the H_2O_2 Oxidation of 2,4,6-Trichlorophenol Catalyzed by Iron Tetrasulfophthalocyanine, J. Am. Chem. Soc. 118 (1996) 7410–7411.

(61) S. Sen Gupta, M. Stadler, C.A. Noser, A. Ghosh, B. Steinhoff, D. Lenoir, C.P. Horwitz, K.W. Schramm, T.J. Collins, Rapid Total Destruction of Chlorophenol Priority Pollutants by Activated Hydrogen Peroxide, Science 296 (2002) 326–328.

(62) J.Á. Pino-chamorro, T. Ditrói, G. Lente, I. Fábián, Detailed Kinetic Study of the Direct Photooxidation of 2,4,6-Trichlorophenol, Journal Photochem. and Photobiol. A Chem. 330 (2016) 71–78.

Figure and table captions

Fig. 1 a) XRD patterns of PC50 TiO_2 and FeOOH/TiO_2 samples (0.14, 1.4 and 2.8 wt.% Fe), b) UV/vis absorption spectra of prepared FeOOH/TiO_2 composites, c) XPS survey spectra of FeOOH/TiO_2 samples (0.14 and 1.4 wt.% Fe), d) XPS Fe 2p spectra of FeOOH/TiO_2 samples (0.14 and 1.4 wt.% Fe).

Fig. 2 a) XRD patterns of 0.14 wt.% Fe/TiO_2 composites calcined at different temperatures, b) UV/vis absorption spectra of 0.14 wt.% Fe/TiO_2 composites calcined at different temperatures, c) TEM image of FeOOH/TiO_2 (0.14 wt.% Fe) calcined at 250^{o}C, d) Raman spectra of 0.14 wt.% Fe/TiO_2 composites calcined at 120 ^{o}C, 250 ^{o}C and 350 ^{o}C.

Fig. 3 a) TOC calibration curve using KHP standards, b) Mineralisation profiles using FeOOH/TiO_2 with different Fe loading, c) A plot of 2,4,6-TCP mineralisation efficiency versus Fe concentration in FeOOH/TiO_2 at 4 h run, d) Mineralisation profiles using FeOOH/TiO_2 (0.14 wt.% Fe) prepared with different Fe (III) precursors.

Fig. 4 a) Mineralisation profiles using 0.14 wt.% Fe/TiO_2 with different calcination temperatures, b) TOC measurement with error bar on optimised FeOOH/TiO_2 after conducting triple experiments, c) Degradation profiles using PC50 TiO_2 and optimised FeOOH/TiO_2 sample monitored by HPLC, d) Comparison of results obtained from TOC, HPLC and UV-vis measurements for TCP degradation using optimised FeOOH/TiO_2 sample.

Fig. 5 a) Mineralisation profiles of 2,4-D using PC50 and FeOOH/PC50 (0.14 wt.% Fe) sample, b) Comparison of results obtained from TOC, HPLC and UV-vis spectrophotometer for 2,4-D degradation using optimised FeOOH/TiO_2 sample.

Fig. 6 a) XRD patterns of the products obtained after calcination of Fe(III) nitrate nonahydrate at different temperatures, b) Enlarged XRD patterns of selected three samples, c) Raman spectra of the products obtained after calcination of Fe(III) nitrate nonahydrate (%) at different temperatures, d) Photoluminescence (PL) spectra of unmodified PC50 TiO_2 and optimised $FeOOH/TiO_2$ sample.

Fig. 7 a) Recycling performance of 0.14 wt.% Fe/TiO_2 samples at different calcination temperatures with normalisation when taking TiO_2 as a reference, b) Effect of different scavengers/additives on 2,4,6-TCP degradation efficiency of $FeOOH/TiO_2$ (0.14 wt.% Fe).

Fig. 8 a & c) HPLC chromatograms showing the degradation profiles of 2,4,6-TCP with $FeOOH/TiO_2$ (0.14 wt.% Fe), b & d) Corresponding ESI-MS chromatograms.

Scheme 1 Proposed reaction scheme for 2,4,6-TCP degradation.

Scheme 2 Proposed mechanism for major charge transfer pathways on $FeOOH/TiO_2$ for degradation of 2,4,6-TCP and 2,4-D.

Table 1 BET surface area analysis for effect of calcination temperature.

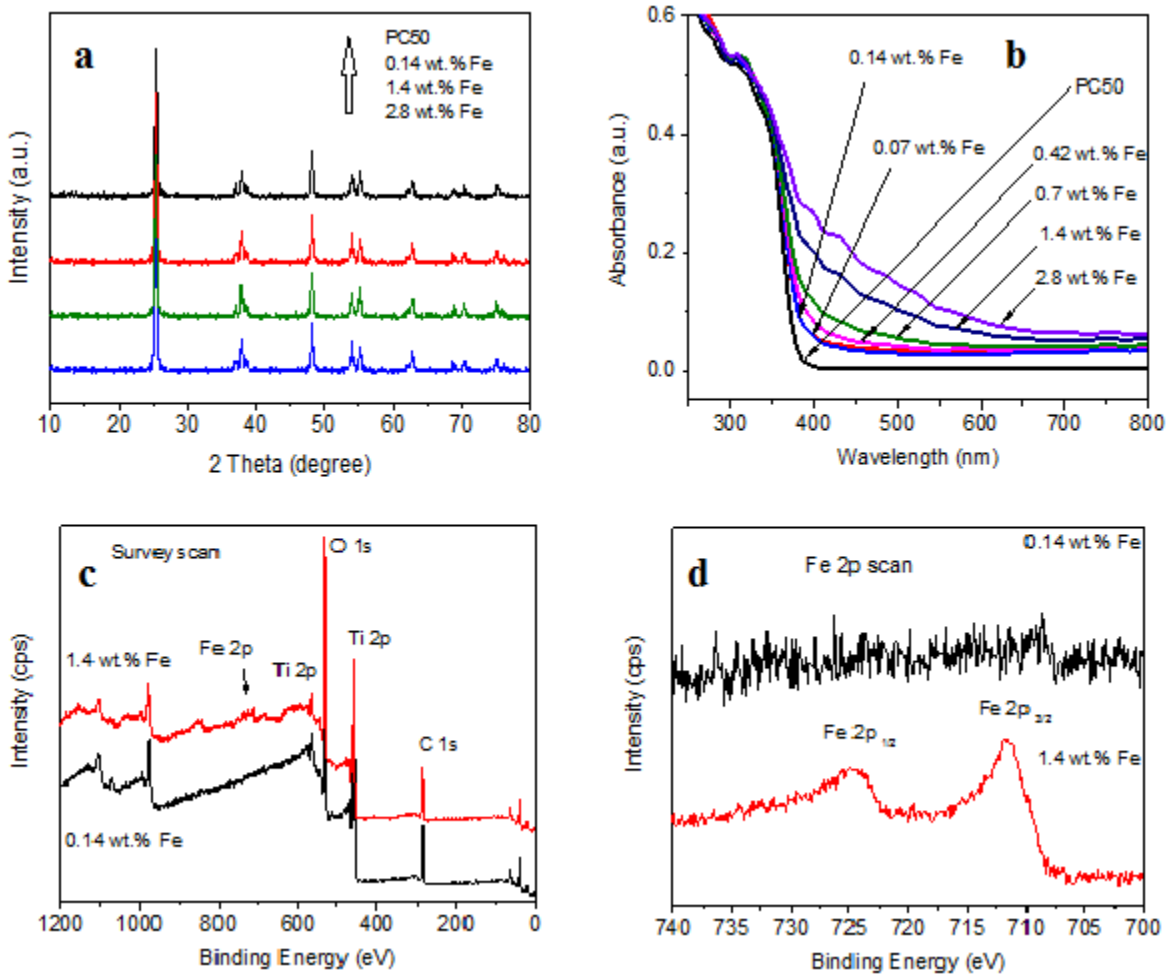

657

658 **Fig. 1** a) XRD patterns of PC50 TiO_2 and FeOOH/TiO_2 samples (0.14, 1.4 and 2.8 wt.% Fe), b)
659 UV/vis absorption spectra of prepared FeOOH/TiO_2 composites, c) XPS survey spectra of
660 FeOOH/TiO_2 samples (0.14 and 1.4 wt.% Fe), d) XPS Fe 2p spectra of FeOOH/TiO_2 samples
661 (0.14 and 1.4 wt.% Fe).

662

663

664

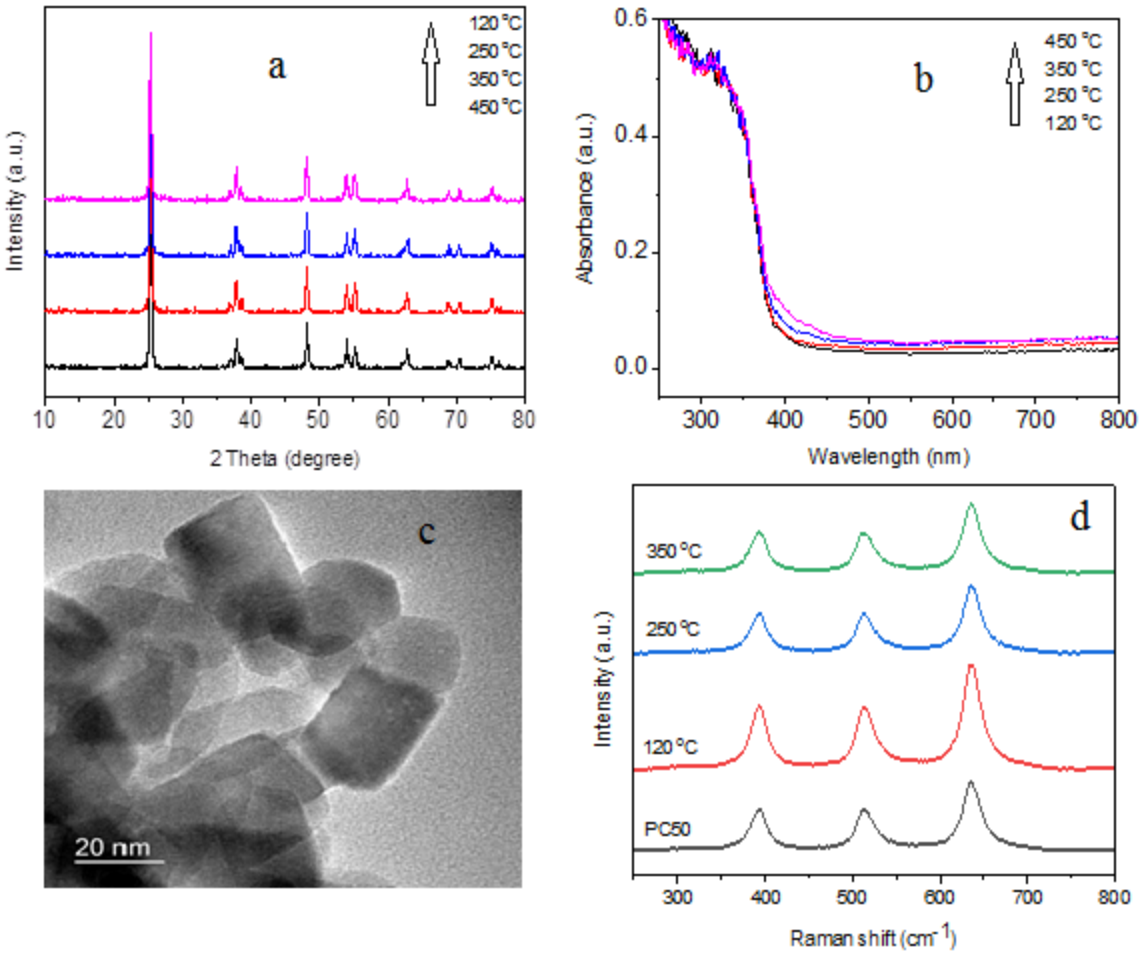

665

666 **Fig. 2** a) XRD patterns of 0.14 wt.% Fe/TiO_2 composites calcined at different temperatures, b)
667 UV/vis absorption spectra of 0.14 wt.% Fe/TiO_2 composites calcined at different temperatures,
668 c) TEM image of FeOOH/TiO_2 (0.14 wt.% Fe) calcined at 250ºC, d) Raman spectra of PC50
669 TiO_2 and 0.14 wt.% Fe/TiO_2 composites calcined at 120 ºC, 250 ºC and 350 ºC.

670

671

672

673

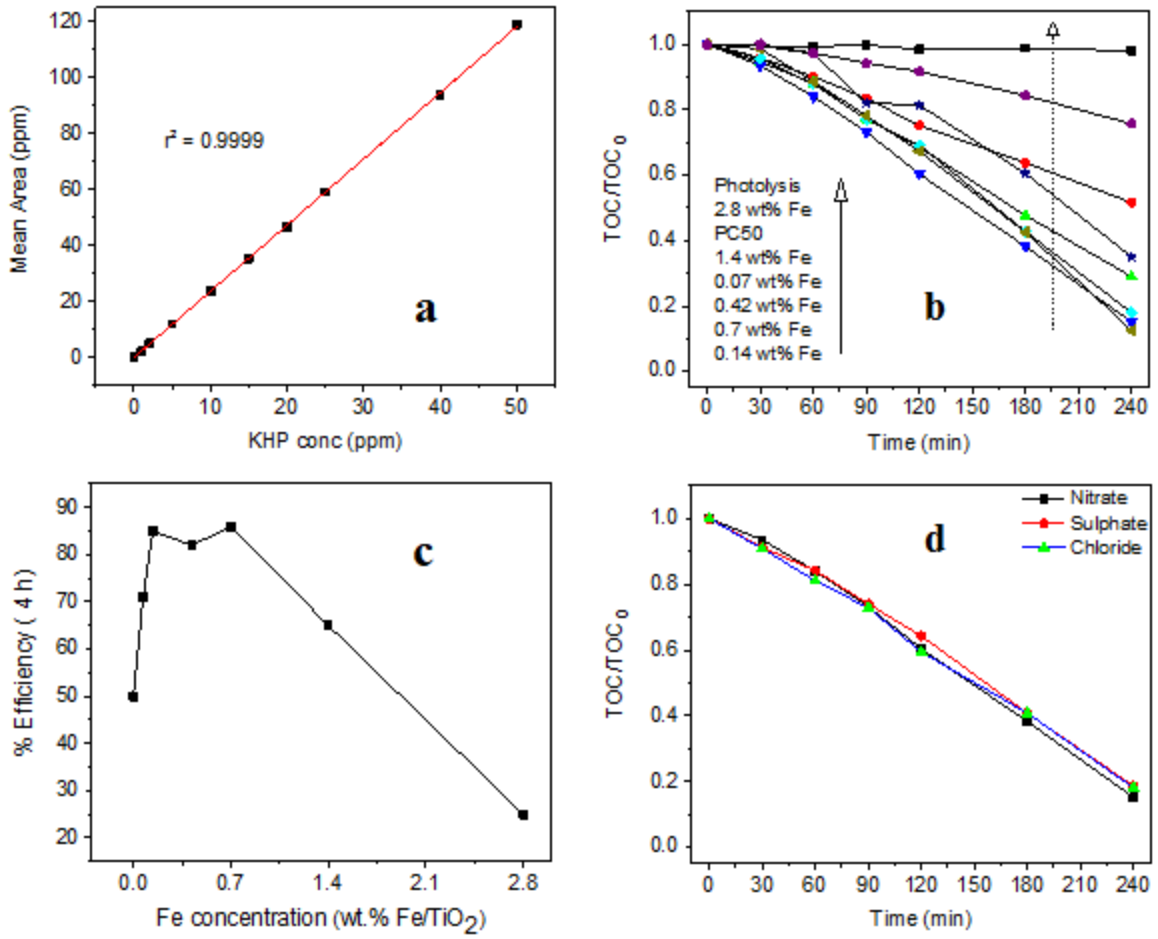

674

675 **Fig. 3** a) TOC calibration curve using KHP standards, b) Mineralisation profiles of TCP using
676 $FeOOH/TiO_2$ with different Fe loading, c) A plot of 2,4,6-TCP mineralisation efficiency versus
677 Fe concentration in $FeOOH/TiO_2$ at 4 h run, d) Mineralisation profiles of TCP using
678 $FeOOH/TiO_2$ (0.14 wt.% Fe) prepared with different Fe (III) precursors.

679

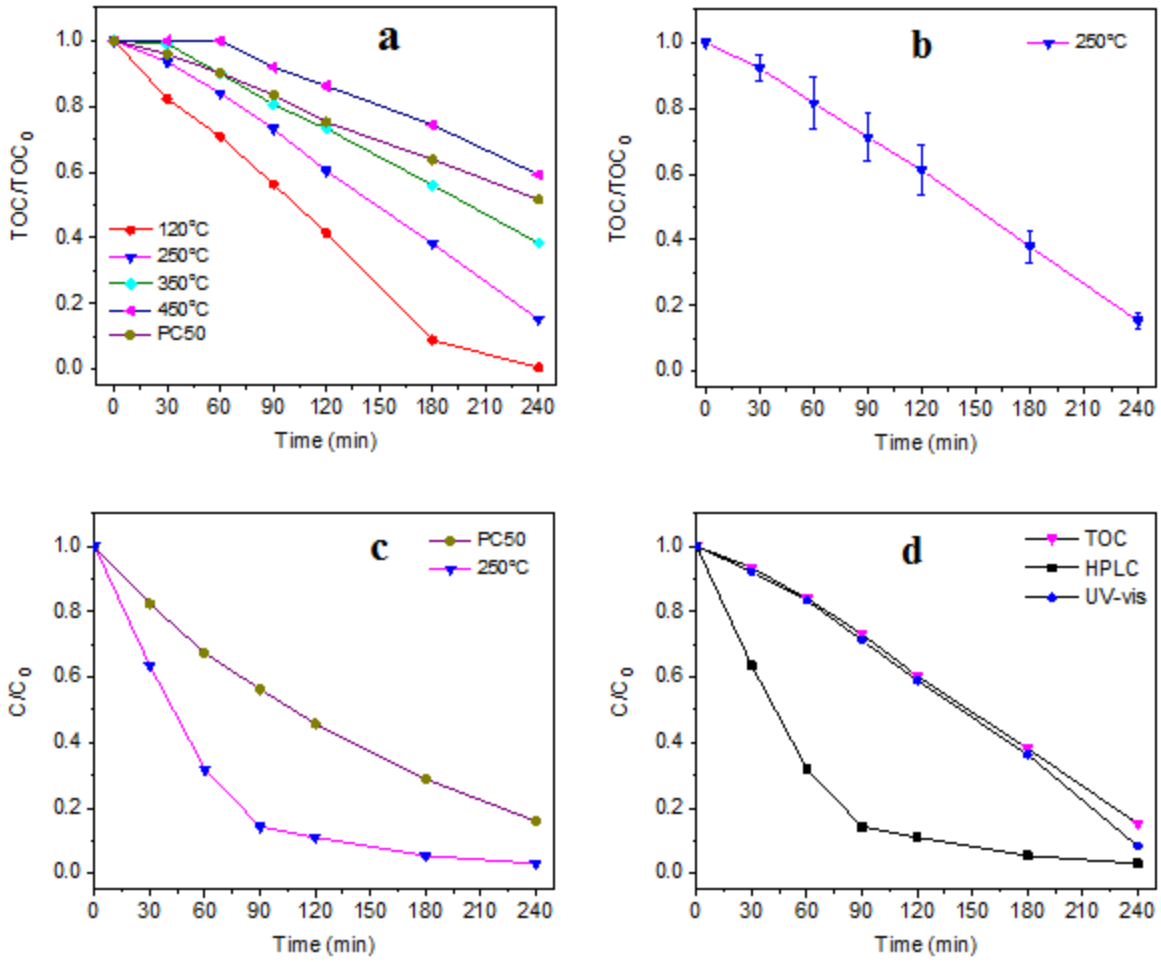

680

681 **Fig. 4** a) Mineralisation profiles of TCP using 0.14 wt.% Fe/TiO_2 with different calcination
682 temperatures, b) TOC measurement with error bar on optimised FeOOH/TiO_2 after conducting
683 triple experiments, c) Degradation profiles of TCP using PC50 TiO_2 and optimised FeOOH/TiO_2
684 sample monitored by HPLC, d) Comparison of results obtained from TOC, HPLC and UV-vis
685 measurements for TCP degradation using optimised FeOOH/TiO_2 sample.

686

687

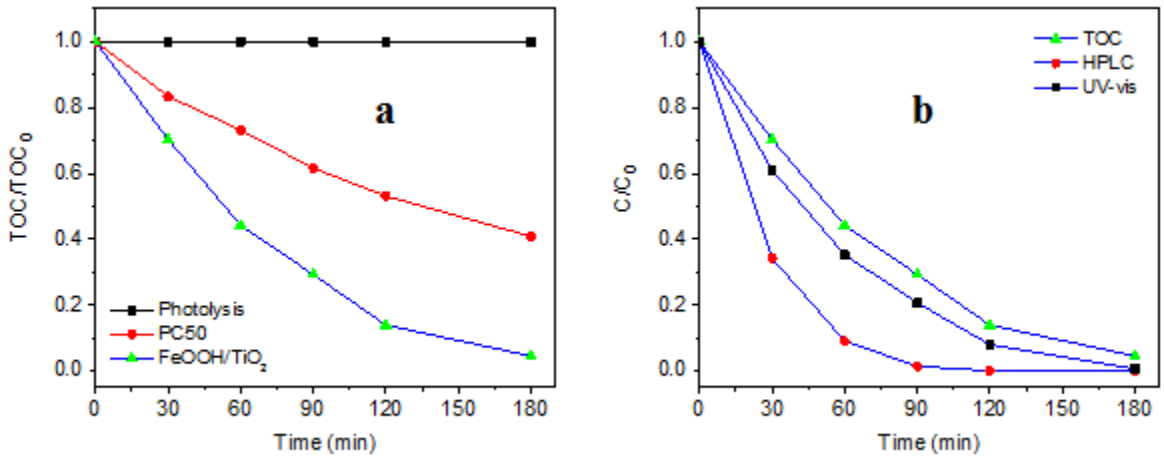

Fig. 5 a) Mineralisation profiles of 2,4-D using PC50 and FeOOH/PC50 (0.14 wt.% Fe) sample, b) Comparison of results obtained from TOC, HPLC and UV-vis spectrophotometer for 2,4-D degradation using optimised FeOOH/TiO_2 sample.

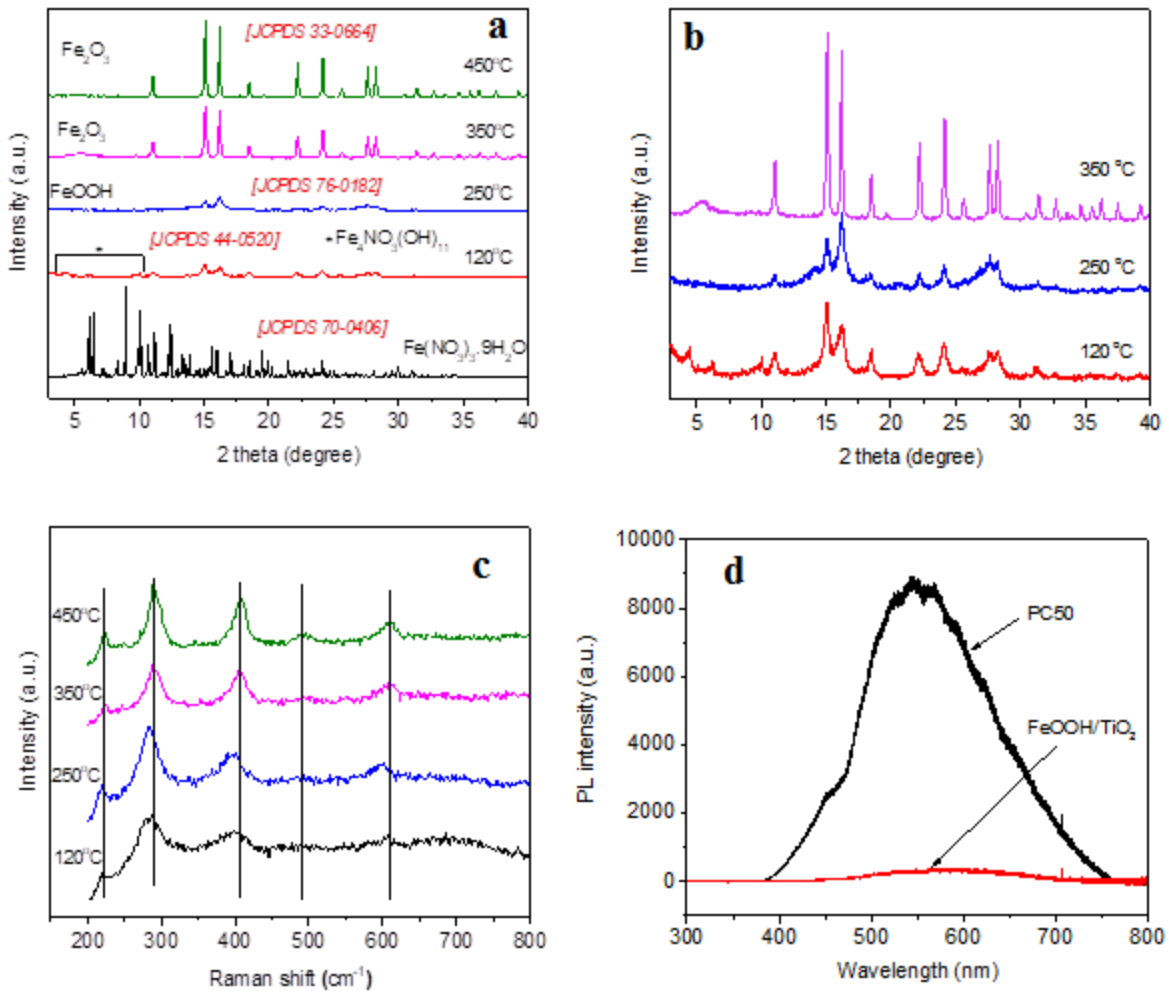

Fig. 6 a) XRD patterns of the products obtained after calcination of Fe(III) nitrate nonahydrate at different temperatures, b) Enlarged XRD patterns of selected three samples, c) Raman spectra of the products obtained after calcination of Fe(III) nitrate nonahydrate (%) at different temperatures, d) Photoluminescence (PL) spectra of unmodified PC50 TiO_2 and optimised $FeOOH/TiO_2$ sample.

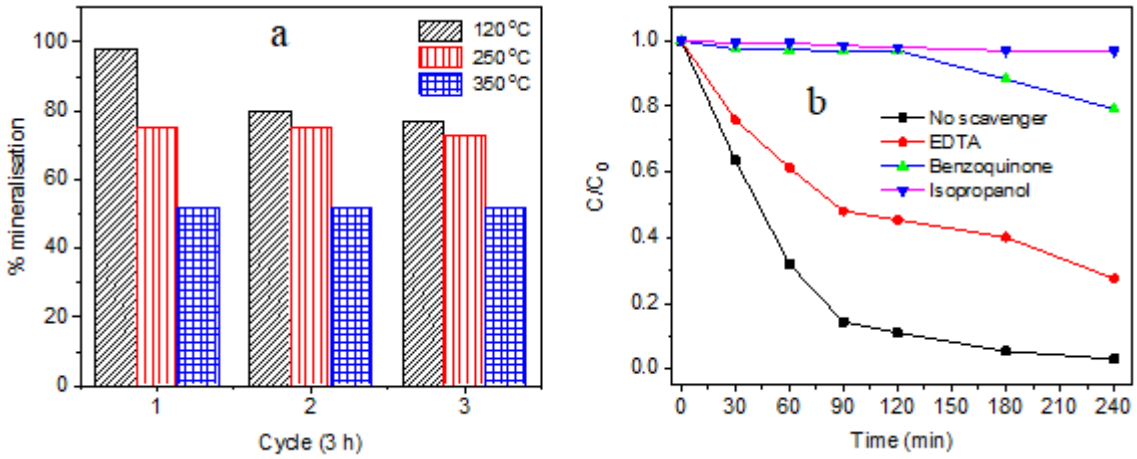

Fig. 7 a) Recycling performance of 0.14 wt.% Fe/TiO_2 samples at different calcination temperatures with normalisation when taking TiO_2 as a reference, b) Effect of different scavengers/additives on 2,4,6-TCP degradation efficiency of FeOOH/TiO_2 (0.14 wt.% Fe).

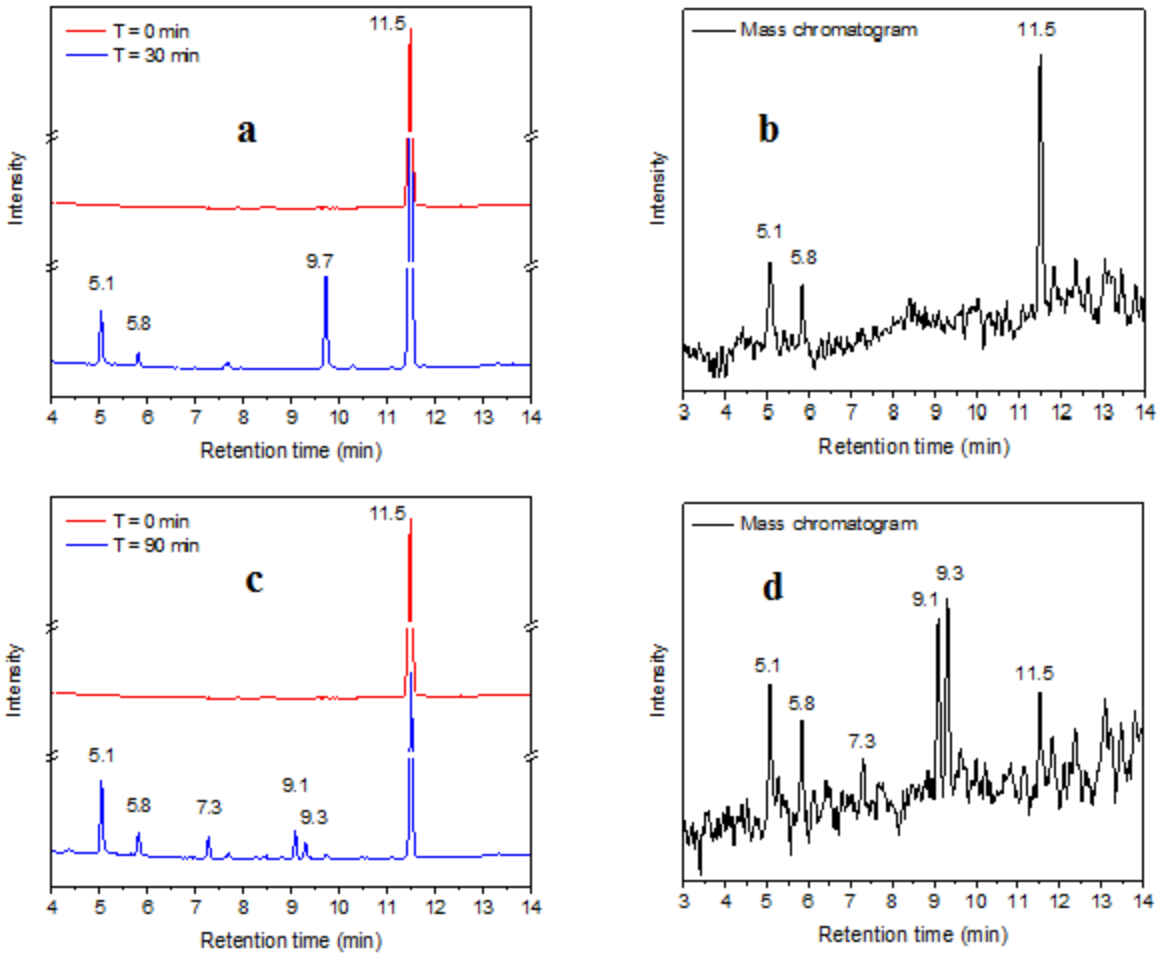

Figs. 8 a & c) HPLC chromatograms showing the degradation of 2,4,6-TCP with FeOOH/TiO_2 (0.14 wt.% Fe), b & d) Corresponding ESI-MS chromatograms.

Scheme captions

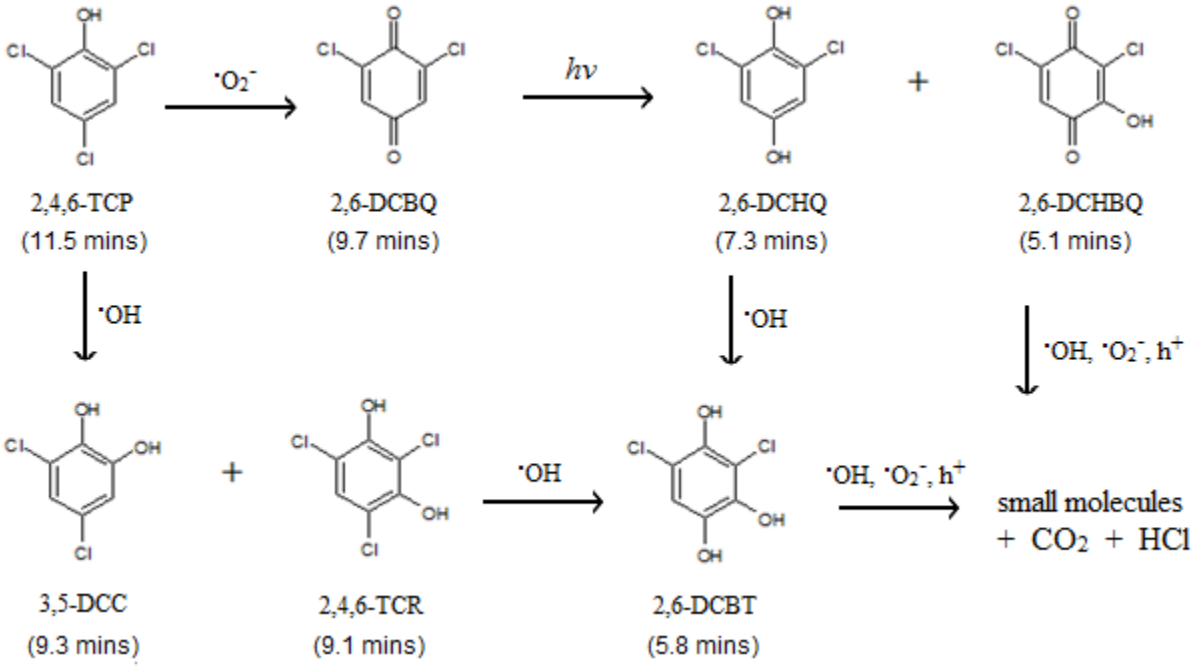

Scheme 1 Proposed reaction scheme for 2,4,6-TCP degradation.

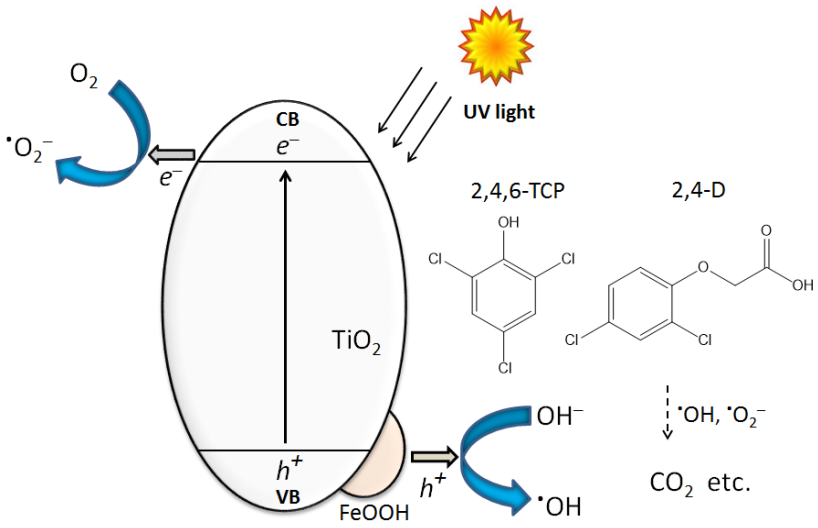

Scheme 2 Proposed mechanism for major charge transfer pathways on FeOOH/TiO_2 for mineralisation of 2,4,6-TCP and 2,4-D.

Table captions

Table 1 BET surface area analysis for effect of calcination temperature.

BET surface area					
Sample	PC50		0.14 wt.% Fe		
	(unmodified)	(120 ºC)	(250 ºC)	(350 ºC)	(450 ºC)
S.A (m^2/g)	47	48	48	49	49